Kinetics and Mechanisms of CO Oxidation on $Nd_{1-x}Sr_xCoO_{3-y}$ Catalysts with Static and Flow Methods

Ha Jun Jung, Jong-Tae Lim, Sung Han Lee,* Yong-Rok Kim,* and Joong-Gill Choi*

Department of Chemistry, Yonsei University, Seoul 120-749, Korea

Received: October 9, 1995; In Final Form: January 31, 1996[⊗]

Perovskite-type $Nd_{1-x}Sr_xCoO_{3-y}$ catalysts with various Sr mole fraction were prepared and investigated for the effect of Sr substitution on their catalytic activities in the oxidation of carbon monoxide. Utilizing the static and flow methods, kinetic studies have been carried out between 373 and 523 K. The initial reaction was investigated by the static reactor system using a differential photoacoustic cell, and for the study of reaction stage showing a constant catalytic activity after an initial stage characterized by high reaction rates, the flow reactor system using on-line gas chromatography was employed. The catalytic activity increased with increasing amounts of Sr substitution for Nd in $NdCoO_3$ compounds, and it also increased with higher reaction temperature within the range of 373−523 K. Kinetic data obtained in an initial reaction stage by CO_2 photoacoustic spectroscopy showed that the reaction partial orders to CO and O_2 were 0.8−0.9 and 0, respectively. In the reaction stage showing a constant catalytic activity after an initial stage, the oxidation was found to be first order with respect to CO and 0.5 order with respect to O_2. The concentration of oxygen vacancy in the solid catalyst was shown to be the controlling factor for the oxidation of carbon monoxide. According to the experimental results, the mechanisms of the CO oxidation processes are discussed, and it is believed that O_2 adsorbs on the oxygen vacancies (V_o^x) formed by Sr substitution while CO adsorbs on the lattice oxygens during the reaction process.

Introduction

Perovskite-type oxides have received a great deal of attention in the area of catalysis because of their catalytic properties in total oxidation processes and their stability in structure.[1−4] The catalytic activity of perovskite oxide has been well-known in association with the formation of an oxygen-deficient structure. In the case of $LaCo_{1-x}O_{3-y}$ system, the chemisorption on this catalyst takes place readily due to the presence of anion vacancies and low-spin Co^{3+} cations in the compound.[3] Perovskite phases show the semiconducting properties induced by isomorphous substitution, which implies that the nonstoichiometry of the perovskite-type $NdCoO_3$ can be varied by the Sr ion substitution for Nd ions. Therefore, it is expected from the Sr substitution that the variation of the oxidation state of cobalt in $Nd_{1-x}Sr_xCoO_{3-y}$, resulting in the concentration change of oxygen vacancy, acts as an important role for the enhancement of the catalytic activity.

Although various absorption spectroscopy techniques can be applied for the study of catalytic reactions, it is difficult to measure directly the change in the concentration of product in the initial reaction stage as a function of time. In this study, photoacoustic spectroscopy is utilized for the initial stage reaction process because of its selectivity and extremely low molecular gas level detection limit, which enable us to obtain a signal with enough intensity for the time-resolved experiments.[5−8]

In the present work, $Nd_{1-x}Sr_xCoO_{3-y}$ systems with a variety of Sr mole fractions were prepared to investigate the effect of Sr substitution on their catalytic activities in the oxidation reaction of carbon monoxide. Kinetic studies for the CO oxidation on the catalysts were carried out using CO_2 laser based photoacoustic spectroscopy and on-line gas chromatography (GC) techniques. Rates of CO_2 formation and the influences of CO and O_2 on the reaction rate in the initial reaction stage were investigated by using a differential photoacoustic cell, and the reaction stage showing a constant catalytic activity after the initial reaction was studied by an on-line gas chromatography system.

Experimental Section

The perovskite-type $Nd_{1-x}Sr_xCoO_{3-y}$ catalysts were prepared from the mixture of $Nd(NO_3)_3{\cdot}6H_2O$, $Sr(NO_3)_2{\cdot}4H_2O$, and $Co(NO_3)_2{\cdot}6H_2O$ (99.9%, Aldrich Co.). The synthesis process is the following: the starting materials were weighed to yield $Nd_{1-x}Sr_xCoO_{3-y}$ sample of various compositions, with $x = 0$, 0.25, 0.5, and 0.75. Each was dissolved in deionized water; then the solutions were mixed. The resulting solutions were heated at 120 °C, with continuous stirring in order to evaporate water, dried, calcined at 1200 °C for 24 h in an alumina crucible, and then cooled to room temperature. To investigate the crystal structure and lattice parameters, X-ray powder diffractometry (XRD) measurements were carried out with a diffractometer (Philips PW 1710) equipped with a curved graphite monochromator in a selected beam path. The present catalysts were found to be cubic structures from their diffraction patterns, but the number of diffraction peaks decreased with increasing x-value, and only five diffraction peaks were observed for the $Nd_{0.5}Sr_{0.5}CoO_{3-y}$ system. The accurate parameters (a-values) determined by the Nelson−Riley method were 7.548, 7.581, 3.811, and 3.820 Å for $NdCoO_3$, $Nd_{0.75}Sr_{0.25}CoO_{3-y}$, $Nd_{0.5}Sr_{0.5}CoO_{3-y}$, and $Nd_{0.25}Sr_{0.75}CoO_{3-y}$, respectively. As reported in the previous paper,[9] it is believed that $NdCoO_3$ and $Nd_{0.75}Sr_{0.25}CoO_{3-y}$ are slightly distorted perovskite structures, while $Nd_{0.5}Sr_{0.5}CoO_{3-y}$ and $Nd_{0.25}Sr_{0.75}CoO_{3-y}$ are simple cubic structures. The mole ratio (τ) of Co^{4+} formed by Sr incorporation was determined by the iodometric titration method. On

* Author to whom correspondence should be addressed.

[⊗] Abstract published in *Advance ACS Abstracts,* May 15, 1996.

S0022-3654(95)02985-6 CCC: $12.00

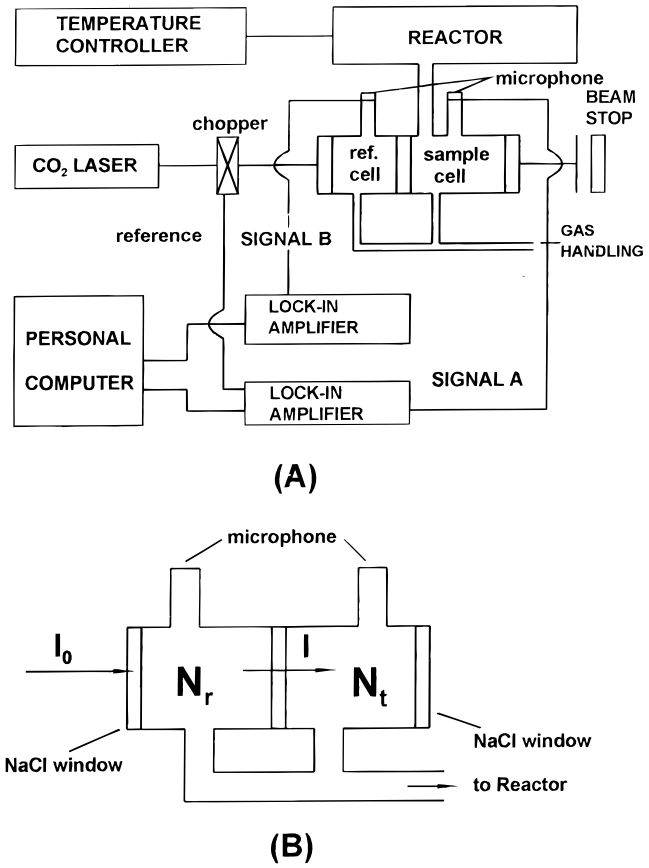

Figure 1. Schematic diagrams of (A) differential photoacoustic experimental setup and (B) differential photoacoustic cell.

the basis of the electroneutrality condition, the *y*-values indicating the oxygen deficiency were calculated from the equation of $y = (x - \tau)/2$, and therefore the resulting nonstoichiometric compositions were determined to be $NdCo^{III}O_{3.00}$, $Nd_{0.75}Sr_{0.25}Co^{III}_{0.92}Co^{IV}_{0.08}O_{2.92}$, $Nd_{0.5}Sr_{0.5}Co^{III}_{0.83}Co^{IV}_{0.17}O_{2.84}$, and $Nd_{0.25}Sr_{0.75}Co^{III}_{0.84}Co^{IV}_{0.16}O_{2.71}$. The BET surface areas of the catalysts used in this work were in the range of 1.5−2.3 m^2/g. The electrical conductivity measurements were performed at 473 K at various CO and O_2 partial pressures. The dc conductivity was measured by means of the four-probe method. The details of the experimental apparatus, instruments, and calculations of measured conductivity have been reported in previous papers.[10,11]

In the present work, photoacoustic spectroscopy was applied to investigate the CO_2 formation in initial catalytic oxidation stage. Figure 1 shows an experimental arrangement for the photoacoustic detection method used in this work. The differential photoacoustic cell consists of two compartments, i.e., reference cell and sample cell, separated from each other by a NaCl window. The reference cell was filled with a gaseous mixture of CO_2 (6.665 Pa) and N_2 (5.325×10^3 Pa), and the sample cell was connected to the microreactor loaded with catalyst, in which the total pressure of gaseous mixture of CO and O_2 was constantly kept at 5.332×10^3 Pa with N_2 buffer gas. Carbon dioxide produced by the catalytic oxidation of carbon monoxide was detected by its photoacoustic signal. Signals from the microphones attached at the reference cell (signal A) and the sample cell (signal B) were detected by a lock-in amplifier (Stanford Research Systems Model SR850), and the signal ratio (A/B) was recorded by a personal computer as a function of time. The photoacoustic cell was a Helmholtz resonator of 1.9 cm in diameter and 3.3 cm in length with an adjoining tube of 1.0 cm in diameter and 10 cm in length. A CO_2 laser (Synrad Series 48-2-115 Laser "D" version) was internally amplitude modulated at audio frequencies by an oscillator. The laser modulation frequency of 18 Hz was tuned to the Helmholtz resonance of the cell, and the output laser wavelength was determined by the diffraction grating angle controlled by a stepping motor. The details of the experimental apparatus and measurements have been given in a previous article.[8]

Kinetic studies using the on-line GC system were carried out in a conventional single-pass fixed-bed type flow reactor operated at 1.013×10^5 Pa. The reactor was quartz tubing with 1.2 cm diameter and 20 cm length. The catalyst was in the middle of the reactor, and the section beyond the catalyst bed in the reactor was filled with alumina beads to reduce the free space. A K-type thermocouple sealed with an alumina tube was placed just above the catalysts in the reactor to control the reaction temperature. A sample of 1.0 g of catalyst was loaded in the reactor, and He gas was used as a diluent gas. The feed flow rate at ambient conditions was 9 mL/min. The catalyst was pretreated at 573 K under the flowing O_2 condition for 30 min after loading into the reactor. The range of reaction temperature studied was 373−523 K. The purity of gaseous oxygen and carbon monoxide was better than 99.99%. The gaseous reactants were purified by passing over a bed of molecular sieve to remove water before introducing them into the reactor. Reaction products were analyzed by a gas chromatograph (Hewlett-Packard 5890) equipped with a thermal conductivity detector and a quadruple mass spectrometer. A Carbosphere column was employed to analyze the gas mixture. Gas compositions were calculated using an external standard gas mixture. Blank runs were performed over inert alumina beads in the absence of catalyst. Throughout the experiments, approximately 1% conversion of carbon monoxide to CO_2 was obtained in the reaction temperature range of 373−523 K.

Results

In the present results, $Nd_{1-x}Sr_xCoO_{3-y}$ ($0 \le x \le 0.75$) oxides showed catalytic activities in CO oxidation in the temperature range from 373 to 523 K. The experimental data showed that Sr doping increases the catalytic activity of the perovskite-type $Nd_{1-x}Sr_xCoO_{3-y}$ system, which indicates that the defects formed in the crystalline sample contribute to the catalytic activity of the sample. The initial reaction stage of the CO oxidation on the fresh surface of catalyst was investigated by photoacoustic spectroscopy. Figure 2 shows the CO_2 photoacoustic signals as a function of time for the initial catalytic oxidation at 473 K, in which signal A was obtained after CO introduction on the oxygen-pretreated $Nd_{0.25}Sr_{0.75}CoO_{3-y}$ catalyst, signal B was obtained after O_2 introduction on CO-pretreated catalyst, and signal C was obtained after the introduction of stoichiometric reactant mixture ($P_{O_2} = 1.33 \times 10^3$ Pa, $P_{CO} = 2.67 \times 10^3$ Pa, $P_{N_2} = 1.33 \times 10^3$ Pa) in the absence of catalyst in the static reactor system. When oxygen was introduced on a CO-preadsorbed catalyst, no CO_2 formation was observed on the catalyst. However, when CO was introduced on an oxygen-preadsorbed catalyst, CO_2 was produced at a high rate. Figure 3 shows the variations of CO_2 photoacoustic signal with P_{CO}/P_{O_2} ratio on $Nd_{0.75}Sr_{0.25}CoO_{3-y}$ catalyst. In the initial reaction stage, the rate of CO_2 formation was not very dependent on P_{O_2}, but largely dependent on P_{CO}. The partial orders with respect to CO and O_2 obtained from the data in Figure 3 were found to be 0.8−0.9 order and zero order, respectively, as listed in Table 1. Figure 4 shows the CO_2 signals measured at the various temperatures, in which the rate of CO_2 formation in the initial stage increases with the increasing temperature in

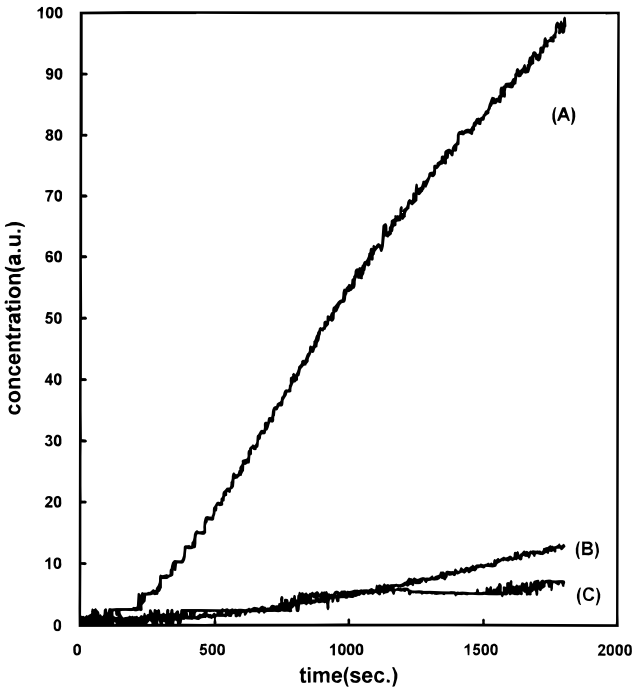

Figure 2. CO_2 photoacoustic signals at 473 K. (A) After CO_2 introduction on $Nd_{0.75}Sr_{0.25}CoO_{3-y}$ catalyst pretreated with oxygen; (B) after O_2 introduction on $Nd_{0.75}Sr_{0.25}CoO_{3-y}$ catalyst pretreated with carbon monoxide; (C) after introduction of stoichiometric mixture of CO and O_2 without catalyst.

TABLE 1: Effect of Partial Pressures of Carbon Monoxide and Oxygen on Initial Rates of CO Oxidation at 473 K over Various Catalysts[a]

	rate $= kP_{CO}^{\alpha}P_{O_2}^{\beta}$	
catalyst	α	β
$NdCoO_3$	0.73	0.02
$Nd_{0.75}Sr_{0.25}CoO_{3-y}$	0.90	0.04
$Nd_{0.50}Sr_{0.50}CoO_{3-y}$	0.88	0
$Nd_{0.25}Sr_{0.75}CoO_{3-y}$	0.76	0.14

[a] Rates were measured by a differential photoacoustic cell. Catalyst = 0.5 g; $P_{CO} + P_{O_2} + P_{N_2} = 5.33 \times 10^3$ Pa.

TABLE 2: Effect of Partial Pressures of Carbon Monoxide and Oxygen on the Oxidation Rate of Carbon Monoxide at 473 K over Various Catalysts[a]

	rate $= kP_{CO}^{\alpha}P_{O_2}^{\beta}$		
catalyst	α[b]	β[c]	E_a[d] (kJ/mol)
$Nd_{0.75}Sr_{0.25}CoO_{3-y}$	1.02	0.46	64.9
$Nd_{0.50}Sr_{0.50}CoO_{3-y}$	0.98	0.48	66.9
$Nd_{0.25}Sr_{0.75}CoO_{3-y}$	1.06	0.48	62.3

[a] Data were obtained by the flow technique. Catalyst = 1.0 g. [b] P_{CO} dependence was measured at a fixed P_{O_2} (1.33×10^3 Pa). [c] P_{O_2} dependence was measured at a fixed P_{CO} (2.67×10^3 Pa). [d] Rates were measured at $P_{O_2} = 1.33 \times 10^3$ Pa and $P_{CO} = 2.67 \times 10^3$ Pa.

the range of 373−523 K. Figure 5 [A] is the Arrhenius plots for the initial reaction of CO oxidation of $NdCoO_3$ and $Nd_{0.75}Sr_{0.25}CoO_{3-y}$, and the plots show linearity. The activation energies obtained from Figure 5 [A] were 29.0 and 30.0 kJ/mol for $NdCoO_3$ and $Nd_{0.75}Sr_{0.25}CoO_{3-y}$, respectively.

For the reaction after an initial reaction stage, kinetic data were obtained by the flow reactor system using on-line gas chromatography. Figure 6 shows the rates of CO_2 formation as a function of P_{CO} at a fixed P_{O_2} over the various catalysts, in which the rates increase with increasing P_{CO}. Figure 7 shows the rates of CO_2 formation as a function of P_{O_2} at a fixed P_{CO}. According to the equation of rate $= kP_{O_2}^{\alpha}P_{CO}^{\beta}$, the partial orders

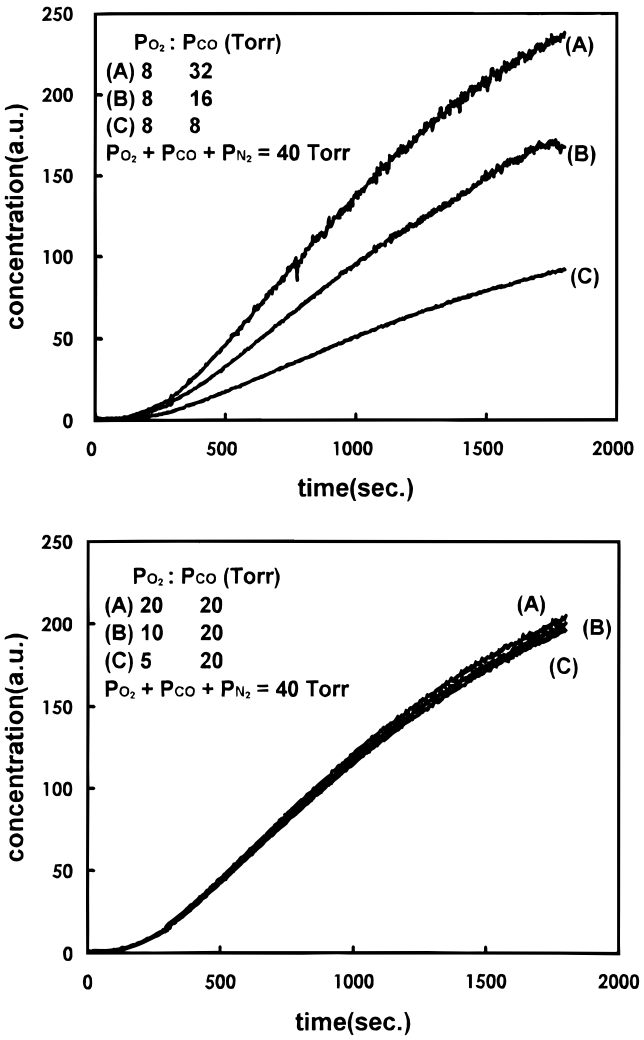

Figure 3. Variations of CO_2 photoacoustic signal with P_{CO}/P_{O_2} ratio for CO oxidation at 473 K on $Nd_{0.75}Sr_{0.25}CoO_{3-y}$.

TABLE 3: Electrical conductivities of $Nd_{1-x}Sr_xCoO_{3-y}$ Catalysts at 473 K under Various Oxygen and Carbon Monoxide Partial Pressures

catalyst	P_{CO} (Pa)	P_{O_2} (Pa)	$\sigma(\Omega\cdot cm)^{-1}$
$NdCoO_3$		1.6	5.0×10^{-1}
$Nd_{0.75}Sr_{0.25}CoO_{3-y}$		1.6	3.0×10^{1}
$Nd_{0.25}Sr_{0.75}CoO_{3-y}$		1.6	5.2×10^{1}
$Nd_{0.5}Sr_{0.5}CoO_{3-y}$		1.6	4.5×10^{1}
$Nd_{0.5}Sr_{0.5}CoO_{3-y}$		3.2×10^3	1.7×10^{1}
$Nd_{0.5}Sr_{0.5}CoO_{3-y}$		6.5×10^3	5.5
$Nd_{0.5}Sr_{0.5}CoO_{3-y}$		1.3×10^4	6.2×10^{-1}
$Nd_{0.5}Sr_{0.5}CoO_{3-y}$	6.5×10^3		1.8×10^{2}
$Nd_{0.5}Sr_{0.5}CoO_{3-y}$	1.3×10^4		5.5×10^{2}
$Nd_{0.5}Sr_{0.5}CoO_{3-y}$	2.6×10^4		4.3×10^{3}

to P_{CO} and P_{O_2} were obtained from the slopes in Figures 6 and 7, and the results are listed in Table 2. As shown in Table 2, the partial orders of CO and O_2 have been found to be 0.98−1.02 and 0.46−0.48, respectively. Figure 5 [B] shows the comparative rates for the two different samples, and the apparent activation energies obtained from the Arrhenius plots were found to be 64.9, 66.9, and 62.3 kJ/mol for $Nd_{0.75}Sr_{0.25}CoO_{3-y}$, $Nd_{0.5}Sr_{0.5}CoO_{3-y}$, and $Nd_{0.25}Sr_{0.75}CoO_{3-y}$, respectively, implying the same mechanism. The data in Table 3 show the electrical conductivities of the catalysts under the various CO and O_2 pressures at 473 K. As shown in Table 2, the conductivity of $Nd_{0.5}Sr_{0.5}CoO_{3-y}$ under CO pressure increased with increasing CO pressure, and the conductivity under O_2 pressure decreased with increasing O_2 pressure.

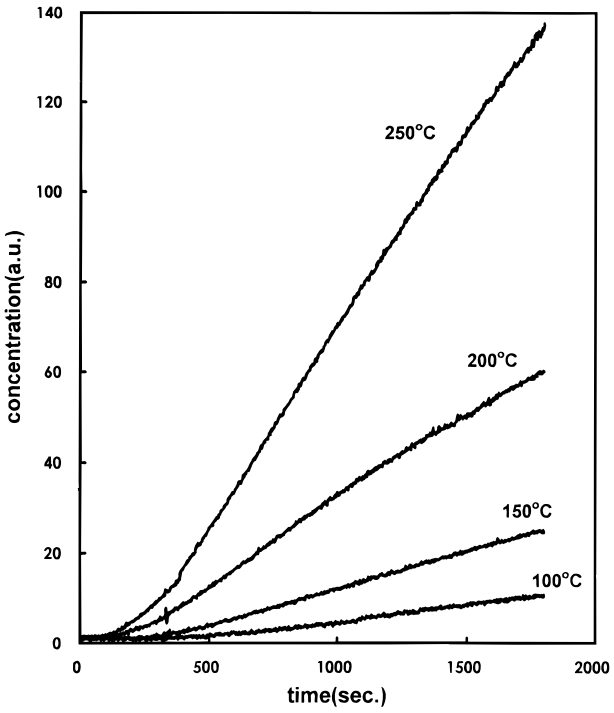

Figure 4. Variations of CO_2 photoacoustic signal with temperature for initial reaction of CO oxidation on $NdSrCoO_{3-y}$.

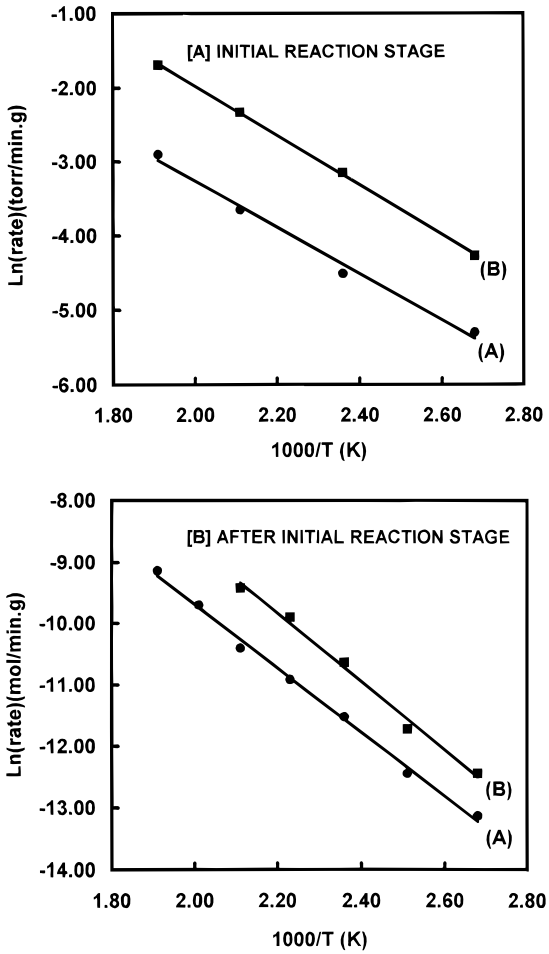

Figure 5. [A] Arrhenius plots for initial reaction of CO oxidation on (A) $NdCoO_3$ and (B) $Nd_{0.75}Sr_{0.25}CoO_{3-y}$ catalyst. [B] Arrhenius plots for CO oxidation on (A) $Nd_{0.75}Sr_{0.25}CoO_{3-y}$ and (B) $Nd_{0.25}Sr_{0.75}CoO_{3-y}$ catalysts after initial reaction (8% CO and 4% O_2 with He balanced to 1.013×10^5 Pa, total flow rate = 9 cm^3/min).

Discussion

From the results of XRD analyses, the present catalysts were found to be perovskite-type structures. When Sr ions are doped into perovskite-type $NdCoO_3$, a part of Co^{3+} ions converts to higher valency (Co^{4+}) based on the principle of controlled valency, and the results of iodometric analyses support this fact. The high valency (Co^{4+}) of cobalt cations is likely to be converted to the low valency (Co^{3+}) since the Co^{4+} is unstable,[12] which results in the formation of oxygen vacancies in the catalyst. This reaction can be represented as

$$Nd_{1-x}Sr_xCo^{III}{}_{1-x}Co^{IV}{}_xO_3 \rightarrow Nd_{1-x}Sr_xCo^{III}{}_{1-x+\delta}Co^{IV}{}_{x-\delta}O_{3-(1/2)\delta} + (\delta/4)O_2 \quad (1)$$

The oxidation rates increased with the Sr substitution for Nd of $NdCoO_3$ as shown in Figures 6 and 7. The results are presented as supporting evidence that the oxygen vacancy in the bulk phase is an important factor controlling the catalytic activity. The oxygen vacancies induced by the Sr doping act as a possible adsorption site for CO or O_2. It is well-known that the oxygen vacancies formed in metal oxide can act as an electron donor and become an adsorption site for oxygen molecule.[13] From the magnitude of the apparent activation energy (62.3−66.9 kJ/mol) in Table 2, it is clear that the reactants can be chemisorbed on the surface of catalyst. It is well-known that the electron transfer during chemisorption causes the formation of a double layer at the surface of catalyst.[14] Since the formation of the double layers donates or withdraws the charge to or from the bands of the catalyst, the electron concentration for the CO oxidation would be controlled by such double layers. Because of O_2 chemisorption on the $Nd_{1-x}Sr_xCoO_{3-y}$ surface, the double layer forming will decrease the density of electrons near the surface, and this low electron density will lower the oxidation rate. In spite of the space charge on the $Nd_{1-x}Sr_xCoO_{3-y}$ surface, the catalytic activity of $Nd_{1-x}Sr_xCoO_{3-y}$ might be enhanced by the Sr doping. The process of the electron transfer during the depletive chemisorption on $Nd_{1-x}Sr_xCoO_{3-y}$ cannot occur infinitely, and equilibrium is established when the potential energy of electrons in the $Nd_{1-x}Sr_xCoO_{3-y}$ becomes equal to that of electrons in the adsorbate. When gaseous oxygen is chemisorbed on the surface of metal oxide, oxygen species can exist in the forms of O_2^-, O_2^{2-}, O^-, and O_3^-.[15] According to the FT-IR study of dioxygen adsorption on reduced cerium oxide by Onish *et al.*,[16] the superoxide species are formed immediately after O_2 introduction and successively converted to O_2^{2-}, O^-, and finally O^{2-}. Superoxide (O_2^-) and peroxide (O_2^{2-}) species can be considered as the intermediates formed during oxygen dissociation, and their existence mainly depends on the basicity of metal oxide and the suitable sites for the stability of the formed species. When the temperature is increased, the formation of O^- becomes more probable.[17,18] If O_2 is adsorbed on an oxygen vacancy defect (Vö − $2e^-$), the reaction can be represented as the following equilibria:

$$O_2(g) + 2e^- \rightleftarrows 2O^-(ads)\ (\text{or } O_2{}^{2-}(ads)) \quad (2)$$

$$O^-(ads) + e^- \rightleftarrows O_o{}^{2-} \quad (3)$$

where e^- is a conduction electron trapped at an oxygen vacancy. The electrical conductivity should decrease with increasing P_{O_2} according to equilibria 2 and 3, which is shown in Table 3. According to the data in Table 2 obtained by the flow technique, the partial orders to O_2 and CO are close to 0.5 order and first

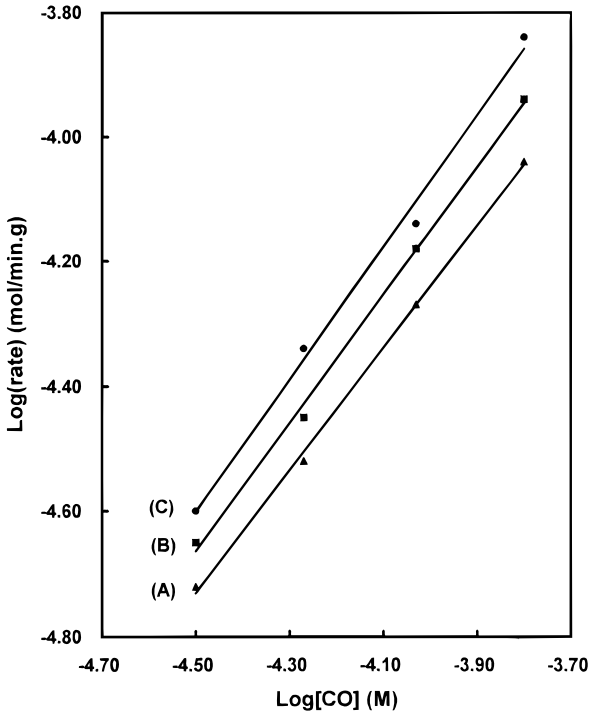

Figure 6. Influence of CO partial pressure on reaction rate for CO oxidation at 473 K on (A) $Nd_{0.75}Sr_{0.25}CoO_{3-y}$, (B) $Nd_{0.5}Sr_{0.5}CoO_{3-y}$, and (C) $Nd_{0.25}Sr_{0.75}CoO_{3-y}$ catalysts.

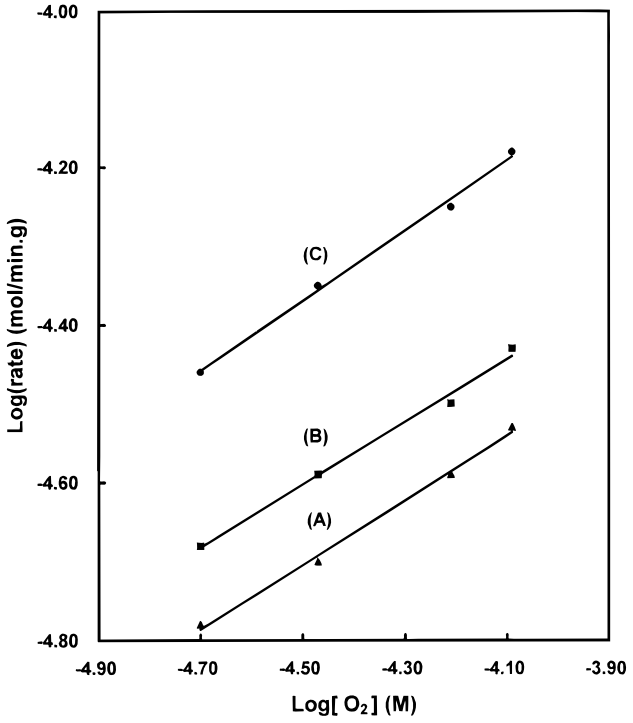

Figure 7. Influence of O_2 partial pressure on reaction rate for CO oxidation at 473 K on (A) $Nd_{0.75}Sr_{0.25}CoO_{3-y}$, (B) $Nd_{0.5}Sr_{0.5}CoO_{3-y}$, and (C) $Nd_{0.25}Sr_{0.75}CoO_{3-y}$ catalysts.

order kinetics, respectively. These results support that the molecular oxygen is dissociatively chemisorbed and CO_2 is formed by the interaction between the adsorbed oxygen and the adsorbed carbon monoxide. Therefore, one must consider that a different site is involved in the adsorption process of CO. The CO_2 photoacoustic signals in Figure 2 show that CO_2 is not significantly produced on the catalyst when the gaseous oxygen is introduced on CO-preadsorbed catalyst, whereas CO_2 is produced at a high rate when gaseous carbon monoxide is introduced on oxygen-preadsorbed catalyst. In general, the reduction of perovskite-type oxides with carbon monoxide leads to the formation of carbonates, and the oxides are not reduced to the metallic state at temperatures below 723 K.[19] According to the study of CO and CO_2 adsorption on $LaCoO_3$ perovskite by Tascon *et al.*,[20] the bidentate carbonate is formed on the surface when CO is introduced at 423 K and the bidentate carbonates are removed from the surface of $LaCoO_3$ above 573 K. The destruction process of bidentate carbonate structures requires considerable activation energy since it includes the oxygen−oxide bond structure.[21] Therefore, in our experiment, it is believed that when the catalyst is pretreated with CO, the bidentate carbonate is formed and does not readily react with oxygen, so that CO_2 photoacoustic signal is not observed at 473 K after the O_2 introduction on CO-preadsorbed catalyst as shown in Figure 2. On the other hand, the preadsorbed oxygen reacts readily with carbon monoxide to form carbon dioxide. If CO is chemisorbed on a lattice oxygens (O_o^{2-}), the reaction can be written as equilibrium 4:

$$CO(g) + O_o^{2-} \rightleftarrows CO_2^{-}(ads) + e^{-} \qquad (4)$$

where CO_2^{-}(ads) is the CO adsorbed on the lattice oxygen. According to equilibrium 4, the electrical conductivity should increase with increasing P_{CO} as in Table 3. CO_2^{-} can be further oxidized to form the bidentate carbonate by equilibrium 5.

$$CO_2^{-}(ads) + O_o^{2-} \rightleftarrows CO_3^{2-}(ads) + e^{-} \qquad (5)$$

Many investigators have proposed that CO is adsorbed on lattice oxygens, and the resulting labile species interact with the adsorbed oxygen to form the more labile monodentate carbonate that decomposes readily, giving CO_2(ads) and O^{-}(ads).[20,22,23] In the initial reaction stage, the partial orders with respect to CO on the various catalysts are in the range of 0.8−0.9 as shown in Table 1. These results make it possible to consider that the reaction obeys a mechanism involving the inhibition process by CO_2 formed during the reaction of CO and O_2 on the catalyst. Then the forward and backward reactions can be represented as the following reactions:

$$CO_2^{-}(ads) + O^{-}(ads) \rightleftarrows CO_3^{2-}(ads) \qquad (6)$$

$$CO_3^{2-}(ads) \rightleftarrows CO_2(g) + O_o^{2-} \qquad (7)$$

According to the experimental data in Table 2 obtained by the single-pass flow reactor system, the partial order with respect to CO is first order, which means that the inhibiting effect of carbon dioxide on the oxidation of carbon monoxide is negligible in the single-pass flow reactor system. The oxidation of carbon monoxide on these catalysts shows 1.5 order in total pressure of reactants, indicating CO_2 formation is increased with increasing partial pressures of CO and O_2. The rate law obtained from the experimental data is rate $= kP_{CO}P_{O_2}^{1/2}$. One can derive the above rate equation from equilibria 2, 4, and 6 and the forward reaction in equilibrium 7. From equilibrium 2,

$$[O^{-}(ads)] = K_2^{1/2}[e^{-}][O_2]^{1/2} \qquad (8)$$

From equilibria 4 and 6, respectively,

$$[CO_2^{-}(ads)] = K_4[O_o^{2-}][CO]/[e^{-}] \qquad (9)$$

$$[CO_3^{2-}(ads)] = K_6[CO_2^{-}(ads)][O^{-}(ads)] \qquad (10)$$

Neglecting the backward reaction in equilibrium 7, the formation

rate of CO_2 can be represented as

$$d[CO_2]/dt = k[CO_3^{2-}(ads)] = kK_6[CO_2^{-}(ads)][O^{-}(ads)] \quad (11)$$

The above rate equation can be rewritten with the substitution of $[CO_2^{-}(ads)]$ and $[O^{-}(ads)]$.

$$d[CO_2]/dt = kK_2^{1/2}K_4K_6[O_o^{2-}][CO][O_2]^{1/2} \quad (12)$$

The concentration of O_o^{2-} can be taken to be constant. Therefore the following equation is consistent with the experimental rate law.

$$d[CO_2]/dt \cong k'[CO][O_2]^{1/2} \quad (13)$$

In the initial reaction stage investigated by the static technique, the oxidation rate was found to be affected by the backward reaction in equilibrium 7, and then the overall reaction orders showed 0.8−0.9 order in the total pressure of the reactants on the catalysts as shown in Table 1: zero order with respect to O_2 and 0.8−0.9 order with respect to CO. The experimental result of zero order with respect to O_2 is obtained from the fact that the O_2 partial pressures do not affect the initial rate. Therefore we are lead to consider that the fresh surface of catalyst is being continuously saturated by oxygen in the initial reaction. If the oxidation is inhibited by the product CO_2 and the reaction rate is not dependent on the oxygen partial pressure, the rate law can be represented as the following:

$$\text{rate} \cong k'(P_{CO}/P_{CO_2})^{\alpha} \qquad 0 \le \alpha < 1 \quad (14)$$

Equation 14 is similar to the rate laws of hydrocarbon oxidation on NiO[24] and ammonia decomposition.[25] The experimental results in Table 1 agree with eq 14 with $0.7 < \alpha < 0.9$.

In conclusion, on the basis of the present results, the rate of O_2 chemisorption is very rapid in the initial reaction stage, but, after the initial reaction stage, the adsorption step of oxygen molecule becomes a rate-determining step. Therefore the concentration of the oxygen vacancy in the $Nd_{1-x}Sr_xCoO_{3-y}$ system is the controlling factor for the oxidation of carbon monoxide.

Acknowledgment. This research was financially supported by the Basic Science Research Institute Program (BSRI, Ministry of Education) and the Korea Science and Engineering Foundation (KOSEF), Republic of Korea.

References and Notes

(1) Meadowcraft, D. B. *Nature* **1970**, *226*, 5248.
(2) Libby, W. F. *Science* **1971**, *171*, 499.
(3) Sorenson, S. C.; Wronkiewics, J. A.; Sis, L. B.; Wirtz, G. P. *Am. Ceram. Soc. Bull.* **1974**, *53*, 446.
(4) Vorhoeve, R. J. H.; Johnson, D. W.; Remeika, Jr. J. P.; Gallagher, P. K. *Science* **1977**, *195*, 827.
(5) Kreuzer, L. B. *Anal. Chem.* **1978**, *50*, 597(A).
(6) Konjevic, N.; Jovicevic, S. *Spectrosc. Lett.* **1979**, *12*, 259.
(7) Jovicevic, S.; Skenderi, S.; Konejevic, N. *Spectrosc. Lett.* **1981**, *14*, 415.
(8) Choi, J. H.; Diebold, G. J. *Anal. Chem.* **1987**, *59*, 519.
(9) Yo, C. H.; Roh, K. S.; Lee, S. J.; Kim, K. H.; Oh, E. J. *J. Kor. Chem. Soc.* **1991**, *35*, 211.
(10) Kim, K. H.; Lee, S. H.; Heo, G.; Choi, J. S. *J. Phys. Chem. Solids* **1987**, *48*, 895.
(11) Park, J. S.; Kim, K. H.; Yo, C. H.; Lee, S. H. *Bull. Kor. Chem. Soc.* **1994**, *15*, 713.
(12) Nitadori, T.; Ichiki, T.; Misono, M. *Bull. Chem. Soc. Jpn.* **1988**, *61*, 621.
(13) Otsuka, K.; Yasui, T.; Morikawa, A. *J. Chem. Soc., Faraday Trans. 1* **1982**, *78*, 3281.
(14) Adamson, A. W. *Physical Chemistry of Surfaces*, 3rd ed.; John Wiley and Sons: New York, 1976; p 196.
(15) Driscoll, D. J.; Martir, W.; Wang, J.-X.; Lunsford, J. H. *J. Am. Chem. Soc.* **1985**, *107*, 58.
(16) Li, C.; Domen, K.; Maruya, K.; Onishi, T. *J. Am. Chem. Soc.* **1989**, *111*, 7683.
(17) Kulkarni, G. U.; Rao, C. N. R.; Roberts, M. W. *J. Phys. Chem.* **1995**, *99*, 3310.
(18) Yang, T.; Feng, L.; Shen, S. *J. Catal.* **1994**, *145*, 384.
(19) Happel, J.; Hnatow, M. *Base Metal Oxide Catalysts*, 1st ed.; Marcel Dekker: New York, 1977; p 117.
(20) Tascon, J. M. D.; Tejuca, L. G. *Z. Phys. Chem. N. F.* **1980**, *121*, 63.
(21) Anderson, J. R.; Boudart, M. *Catalysis Science and Technology*, 3, 1st ed.; Springer-Verlag: New York, 1982; Vol. 3, p 39.
(22) Hertl, W. *J. Catal.* **1973**, *31*, 231.
(23) Yanagisawa, Y.; Takaoka, K.; Yamake, S.; Ito, T. *J. Phys. Chem.* **1995**, *99*, 3704.
(24) Kummer, J. T.; Yas, Y. F. Y. *J. Catal.* **1973**, *28*, 124.
(25) Anderson, J. R.; Boudart, M. *Catalysis Science and Technology*; Springer-Verlag: New York, 1981; Vol. 1, p 115.

JP952985Q